Analyst

RSC Publishing

PAPER

View Article Online
View Journal | View Issue

Cite this: *Analyst*, 2013, **138**, 3201

A high performance non-enzymatic glucose sensor based on nickel hydroxide modified nitrogen-incorporated nanodiamonds†

Chih-Yu Ko,[ac] Jin-Hua Huang,*[a] Supil Raina[b] and Weng P. Kang[b]

Received 13th November 2012
Accepted 22nd March 2013

DOI: 10.1039/c3an36679k

www.rsc.org/analyst

A highly selective, sensitive, and stable non-enzymatic glucose sensor based on Ni hydroxide modified nitrogen-incorporated nanodiamonds ($Ni(OH)_2$-NND) was developed. The sensor was fabricated by e-beam evaporation of a thin Ni film on NND followed by the growth of $Ni(OH)_2$ using an electrochemical process. It was found that the Ni film thickness greatly affects the morphology and electro-catalytic activity of the as-synthesized electrode for non-enzymatic glucose oxidation. Owing to its nanostructure characteristics, the best sensor fabricated by 150 nm Ni deposition showed two wide response ranges, namely, 0.02–1 mM and 1–9 mM, with sensitivities of 3.20 and 1.41 mA mM^{-1} cm^{-2}, respectively, and a detection limit of 1.2 μM ($S/N = 3$). The sensor also showed good long-term stability as well as high selectivity in the presence of interferences such as ascorbic acid, acetaminophen, and uric acid. This finding reveals the possibility of exploiting the NND as an electrochemical biosensor platform where high performance addressable sensor arrays could be built.

Introduction

The detection of glucose is extremely important in many realms such as medicine, biotechnology, and food industry. Accurate, fast, and reliable measurement of glucose is greatly needed, especially in clinical diagnostics. Therefore, much effort has been devoted for more than two decades to the development of electrocatalytic glucose sensors.[1,2] The most common glucose biosensors, enzymatic type, based on immobilization of glucose oxidase (GOx) onto various substrates have demonstrated some useful applications.[3–7] However, the major problem for this type of oxidase-based sensor is poor stability arising from the loss of enzyme activity during the immobilization process and even in the storage period, which impairs sensitivity and reproducibility of these sensors.[3] Another drawback is the high operating potential that leads to limited selectivity of glucose in blood samples in the presence of uric acid (UA), acetaminophen (AC), and ascorbic acid (AA).[8] As a result, many elaborate fabrication and immobilization techniques are required to overcome these issues. Because of the above-mentioned problems of enzymatic GOx sensors, non-enzymatic sensors have received increasing interest in recent years.

Various noble metals (*e.g.* Pt, Au, Ni and Cu), alloys (*e.g.* Pt–Pb), and oxides (*e.g.* NiO, $Ni(OH)_2$ and CuO) have been investigated in the development of effective non-enzymatic glucose sensors.[9] In general, bulk metal based electrodes (in particular Pt and Au) show low sensitivity and poor selectivity caused by the slow kinetics due to limited surface area, and suffer heavily from surface fouling due to adsorbed intermediates and chloride ions.[2,10] In contrast, conventional (*i.e.*, unmodified) carbon electrodes such as carbon nanotubes (CNT) and diamond[11,12] exhibit low background signal and high fouling resistance owing to the chemically inert nature of carbons, which, unfortunately, weakens their catalytic ability as compared to metals. A common approach for addressing these problems is to employ a structured (micro- or nano-) surface. For instance, the aforementioned drawbacks with the bulk Pt-based electrodes can be greatly improved by introducing a nanoporous Pt film,[13] Pt–Pb nanowire array,[14] *etc.* Similarly, the detection of glucose with sensitivity as high as 1.04–7.32 mA mM^{-1} cm^{-2} has been demonstrated with the nanoscale Ni-based electrodes in the forms of nanoflakes,[15] nanowire arrays,[16] and nanoparticles.[17] These nanostructured metal electrodes possess very high active surface areas, thus favoring kinetically controlled sluggish reactions (the electro-oxidation of glucose) to a greater extent than the diffusion-controlled reactions (the electro-oxidation of interfering species).[18,19]

Another common approach for getting a catalytic electrode with high active surface area is the fabrication of the nanoscale catalytic metal directly onto a nanostructured support (*i.e.*, the nanocomposite electrode).[20–23] Novel carbon nanomaterials such as carbon nanotubes, micro- and nano-diamond, and

[a]*Department of Materials Science and Engineering, National Tsing Hua University, Hsinchu 300, Taiwan. E-mail: jihhuang@mx.nthu.edu.tw; Fax: +886-3-5722366; Tel: +886-3-5162228*

[b]*Electrical Engineering and Computer Science, Vanderbilt University, Nashville, TN 37235, USA*

[c]*Advanced Packaging Technology Department, ITRI, Hsinchu 31040, Taiwan*

† Electronic supplementary information (ESI) available: Supporting figures and the study on the effect of NaOH concentration on the response of glucose. See DOI: 10.1039/c3an36679k

graphene have been shown to be ideal for catalyst and enzyme supports.[7,21–25] Among them, diamond is found to be the most stable in a wide variety of solutions, thereby providing a robust platform for *in vivo* and *in vitro* applications.[26] The intrinsic diamond consists of a network of strongly bonded sp^3 C–C bonds and has poor electrical conductivity. To make diamond electrically conductive, micro- and even nano-crystalline films have been synthesized with defects and sp^2 bonded structures or doped with impurities.[27] Boron is a p-type dopant while nitrogen incorporation imparts n-type characteristics to diamond. The detection of glucose using nickel hydroxide ($Ni(OH)_2$) modified boron-doped diamond (BDD) electrodes has shown excellent sensitivity (up to 1.04 mA mM^{-1} cm^{-2}), high selectivity, and surface fouling resistance.[22] However, this sensor lacked long-term storage stability (94% loss of sensitivity after 14 days of storage) due to weak adhesion of $Ni(OH)_2$ to the underlying BDD. On the other hand, nitrogen-incorporated nanodiamond (NND) with unique 'ridge' morphology has been found to possess excellent structure stability and electrochemical behavior.[28–30] In this work, the NND film with its highly nanostructured, electrochemically active surface was utilized for the attachment of nanoscale $Ni(OH)_2$ with strong adhesion. The resulting $Ni(OH)_2$ modified NND herein as an electrode for glucose detection has shown excellent sensitivity (up to 3.20 mA mM^{-1} cm^{-2}) and long-term stability (15% loss of sensitivity after 60 days of storage), as well as high selectivity in the presence of interferents such as ascorbic acid (AA), acetaminophen (AC), and uric acid (UA).

Experimental

Chemicals and reagents

Sodium hydroxide (NaOH, 98% purity) and sulfuric acid (H_2SO_4, 97% purity) were used as received from SHOWA. Hydrogen peroxide (H_2O_2, 30 wt%) was obtained from J. T. Baker. D-Glucose ($C_6H_{12}O_6$, 99.5% purity), ascorbic acid ($C_6H_8O_6$, 98% purity), acetaminophen ($C_8H_9NO_2$, 98% purity), and uric acid ($C_5H_4N_4O_3$, 98% purity) were purchased from Sigma-Aldrich. Pure water (~18 MΩ cm) was exclusively used in all aqueous solutions and rinsing procedures.

Preparation of the $Ni(OH)_2$-NND electrodes

The NND film on a highly conductive n-type silicon substrate was grown by microwave plasma-enhanced chemical vapor deposition. The parameters of growth were: power = 1 kW, pressure = 25 torr, temperature = 850 °C, time = 4 h, and a gas mixture of $H_2/CH_4/N_2$ in the ratio of 9 : 1 : 1.[29] Prior to Ni modification, the NND films were cleaned in an acid solution ($H_2O_2 : H_2SO_4 = 1 : 4$) at 80 °C to remove impurities and washed with pure water. Then, each of the NND films was partially sealed using PI adhesive tape purchased from 3M to define an active area of 0.5 cm^2, and a Ni film with a thickness of 50, 100, 150, 200 or 250 nm was deposited onto the as-patterned NND film by electron-beam evaporation. Thereafter, various Ni-coated NND films were used as the working electrodes in a three-electrode cell, with platinum as the counter electrode and Ag/AgCl (saturated KCl) as the reference electrode. A 0.1 M NaOH aqueous solution and cyclic voltammetry, between 0.1 and −0.6 V, at a scan rate of 10 mV s^{-1} were employed for the growth and stabilization of $Ni(OH)_2$. The cyclic scans were repeated until no further increase in the anodic and cathodic peaks was observed.

Characterization and apparatus

All electrochemical measurements were performed using an EG&G 2273 potentiostat in a standard three-electrode cell. A platinum wire, a saturated calomel electrode (SCE), and the $Ni(OH)_2$ modified NND films (area of 0.5 cm^2) on Si were used as the counter, reference, and working electrodes, respectively. All operational potential values were referenced to the SCE. Cyclic voltammetry (CV) analyses and chronoamperometric measurements were carried out under steady-state conditions in a quiescent solution of 0.5 M NaOH at the desired operating potentials. Field-emission scanning electron microscopy (FESEM) was used to characterize the surface morphology of NND before and after modification with $Ni(OH)_2$. In addition, the elemental composition of the as-prepared $Ni(OH)_2$-NND hybrids was acquired using a high-resolution X-ray diffractometer (Bruker D8 SSS).

Results and discussion

Structural characterization

The as-synthesized NND films formed uniform and conformal layers on the highly conductive n-typed silicon substrates as seen in the low-magnification FESEM image (Fig. 1(a)). The NND film consists of two characteristic features, ridged sheets or platelets and nanoparticles on the side-walls and in between them. These features can be seen more prominently in the high-magnification image (Fig. 1(b)). Such a hybrid diamond microstructure can be attributed to the two competing processes of nucleation/growth and plasma-etching of the nanodiamond film. The Raman spectrum obtained from the previous study[28] depicts the characteristic diamond peak (sp^3 hybridized carbon) and graphitic peak (sp^2 hybridized carbon). Also, a shoulder at 1140 cm^{-1} was observed, which is associated with films containing the nanocrystalline phase.

Fig. 2(a)–(c) show the FESEM images of NND films coated with 100, 150, and 200 nm-thick Ni, respectively, by e-beam

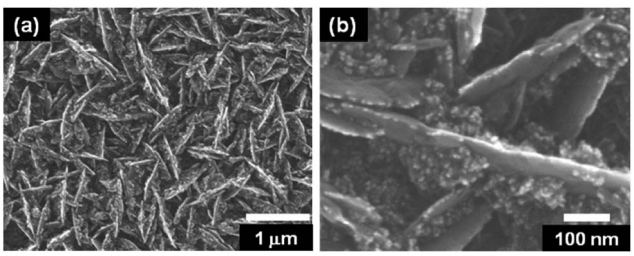

Fig. 1 FESEM images of a NND film showing the "ridge" surface morphology with nanoparticles on and in between the side-walls: (a) low magnification and (b) high magnification.

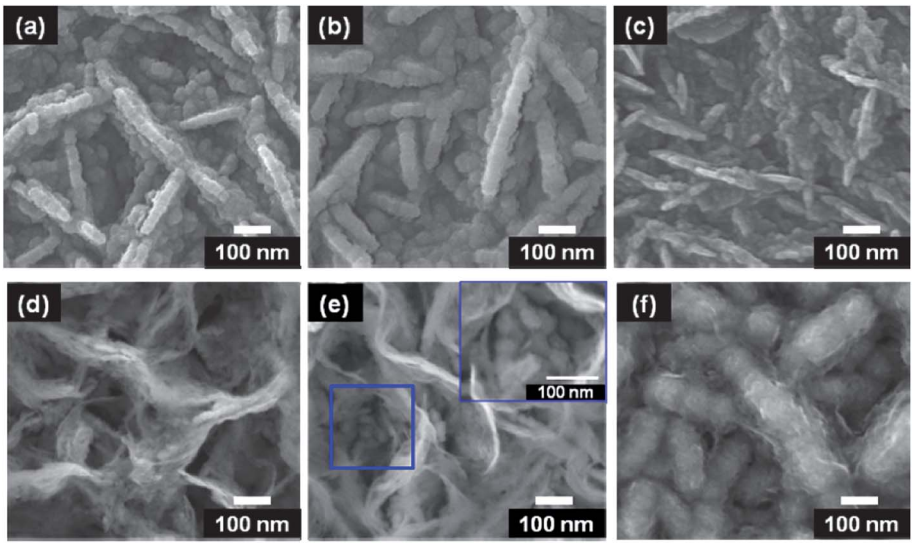

Fig. 2 FESEM images of the as-deposited (a) 100, (b) 150, and (c) 200 nm Ni coated NND films. The corresponding FESEM images after the reaction to form $Ni(OH)_2$ are shown in (d), (e), and (f), respectively.

deposition. Macroscopically, the morphology of the 100 and 150 nm Ni coated samples reveals a uniform and conformal coverage of Ni on both the NND ridges and nanoparticles. As the Ni thickness is varied from 100 to 150 nm, the dimension of Ni coated NND ridges increases marginally but the size of the nanoparticles is enlarged dramatically with an average increment of ~40 nm in diameter. As for the 200 nm Ni coated NND, the structure feature of primitive NND is replaced by a continuous and flat Ni film with some Ni decorated ridged sheets. It is obvious that as the Ni coating thickness is increased above 150 nm, the sheet–nanoparticle hybrid structure transits to a much planar morphology. Fig. 2(d)–(f) show the FESEM images of the 100, 150, and 200 nm Ni coated NNDs after growth of $Ni(OH)_2$ in 0.1 M NaOH by consecutive CVs at a scan rate of 10 mV s^{-1}. Fig. 2(d) and (e), both the 100 and 150 nm $Ni(OH)_2$-NND samples, show adhesion of $Ni(OH)_2$ with sponge-like structures on NNDs. In addition, the 150 nm $Ni(OH)_2$-NND has a greater number of $Ni(OH)_2$ nanoparticles aggregated inside the pores of sponge-like NND. However, the 200 nm $Ni(OH)_2$-NND, Fig. 2(f), demonstrates a relatively flat morphology comprised of a large amount of $Ni(OH)_2$ wrapped grains.

The elemental composition of the as-prepared $Ni(OH)_2$-NND was obtained by high-resolution X-ray diffraction (HRXRD) analysis. The HRXRD pattern (and its assignment) of the as-prepared 150 nm $Ni(OH)_2$-NND is illustrated in Fig. S1,† which shows both the NiO and $Ni(OH)_2$ signatures in addition to the XRD signals generated by the substrate background, including diamond, graphite and unoxidized Ni. The diffraction peaks corresponding to NiO and $Ni(OH)_2$ are relatively broad and weak, which may result from the poor crystallinity and small grain size of NiO and $Ni(OH)_2$. Therefore, a mixture of NiO and $Ni(OH)_2$, instead of pure $Ni(OH)_2$, has been grown on the NND surface. Similar findings have been observed in our previous study[25] on the CNT–Ni hybrid with high-resolution X-ray photoelectron spectroscopy. The growth of NiO may be due to the dehydration of the electrodes while being kept in a dry storage.

The reaction of Ni to $Ni(OH)_2$ has been investigated by many groups.[31–34] Fig. S2† shows an overlay of cyclic voltammograms (CVs) obtained with the 100 nm Ni coated NDD during the growth of $Ni(OH)_2$ by consecutive CV scans, which is in agreement with the literature.[22] In the consecutive CV scans, the evolution of anodic and cathodic peaks is due to the growth of α-$Ni(OH)_2$ and its transformation to the much stable phase, β-$Ni(OH)_2$. The anodic peaks are attributed to α-$Ni(OH)_2$ and β-$Ni(OH)_2$ which are oxidized to γ-NiOOH and β-NiOOH, respectively, while the cathodic peaks are ascribed to γ-NiOOH and β-NiOOH which are reduced to α-$Ni(OH)_2$ and β-$Ni(OH)_2$, respectively. The different morphologies as observed for the $Ni(OH)_2$-NND samples with Ni thickness below and above 150 nm can be ascribed to the specific diffusion behavior of OH^- with the structured electrode surfaces.

Electrocatalytic oxidation of glucose

Before serial studies of glucose sensing, the electrocatalytic oxidation of glucose at the $Ni(OH)_2$-NND electrodes was examined by cyclic voltammetry. Fig. 3(a) shows the CVs of the 150 nm $Ni(OH)_2$-NND electrode in 0.1 M NaOH solution containing 0.5 mM glucose at various scan rates in the range of 5–30 mV s^{-1}. It can be seen that the anodic and cathodic oxidation currents increase with increasing scan rate. Moreover, as shown in the inset of Fig. 3(a), the peak currents for both the anodic and cathodic oxidations of glucose are linearly correlated with the square root of scan rate, implying that the reaction is a classic kinetics-controlled electrochemical process.[14,15,35] The electrochemical response of the 150 nm $Ni(OH)_2$-NND electrode to different concentrations of glucose was also investigated by CV at a scan rate of 10 mV s^{-1}. Fig. 3(b) shows that by increasing the glucose concentration, the oxidation peak current is increased and the potential is shifted to a more positive value. As revealed in the literature,[36,37] the electro-oxidation of glucose

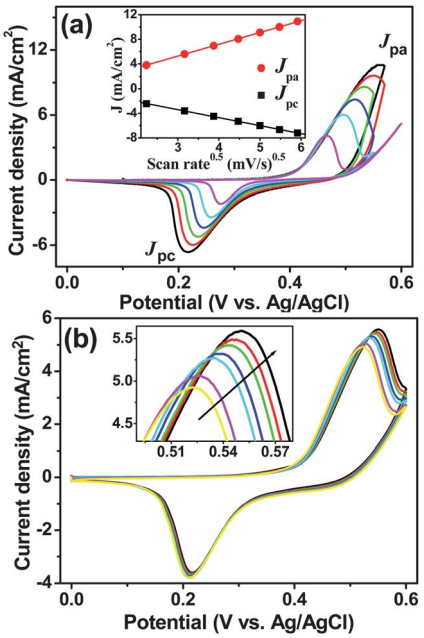

Fig. 3 (a) Cyclic voltammograms of 500 μM glucose obtained with the 150 nm $Ni(OH)_2$-NND electrode in 0.5 M NaOH solution at scan rates of 5, 10, 15, 20, 25, 30 mV s^{-1}. Inset: plot of the peak current density *versus* the square root of scan rate; (b) Cyclic voltammograms of the 150 nm $Ni(OH)_2$-NND electrode at a scan rate of 10 mV s^{-1} in 0.5 M NaOH in the presence of 50, 100, 150, 250, 350, and 500 μM of glucose. Inset: an expanded view of the anodic current density variation in the potential window of 0.49–0.58 V.

to glucolactone was electrocatalyzed by the $NiO(OH)/Ni(OH)_2$ redox couple according to the following reactions:

$$Ni(OH)_2 + OH^- \rightarrow NiO(OH) + H_2O + e^-$$

$$NiO(OH) + \text{glucose} \rightarrow Ni(OH)_2 + \text{glucolactone}$$

Glucose is oxidized by the NiO(OH) species on the electrode surface rapidly at the anodic potential, at the same time converting the NiO(OH) species to $Ni(OH)_2$ ones. In Fig. 3(b), it can be also seen that the cathodic peak current decreases slightly with increasing glucose concentration while undergoing no obvious potential shifts. The changes in the concentrations of the NiO(OH) and $Ni(OH)_2$ species cause the increase of the anodic peak current and the decrease of the cathodic peak current. This phenomenon indicates the irreversible electrocatalysis of glucose and the catalytic conversion of NiOOH to $Ni(OH)_2$ prior to electrochemical reduction. This result also exhibits the excellent elctrocatalytic ability of Ni-NND to glucose oxidation.

Chronoamperometry and optimization of the $Ni(OH)_2$-NND electrode

To achieve the optimum response of the $Ni(OH)_2$-NND electrode, various factors (such as Ni thickness, applied potential, and NaOH concentration) having great influence on the catalytic oxidation behavior of glucose were investigated by amperometry. The effect of NaOH concentration (0.05, 0.1, 0.5, and 1 M) on the response of glucose was studied first and is shown in the ESI.† The results demonstrated that 0.5 M NaOH is the most appropriate solvent to achieve the lowest background current with superior glucose detection signal and was chosen for subsequent experiments.

Next, the effects of Ni thickness in the range of 50–250 nm and applied potential in the range of 0.4–0.55 V were investigated. The amperometric responses of the sensors upon each successive addition of 200 μM glucose were recorded in 0.5 M NaOH solution at various applied potentials, and the results are displayed in Fig. S3.† In the case of the 100 nm $Ni(OH)_2$-NND electrode, a potential of 0.5 V produces the best response, with a linear sensitivity of 3.2 mA mM^{-1} cm^{-2} over the range of 200–1800 μM, as compared to other potentials. According to the sensitivity value, the signal-to-noise ratio (S/N) in 200 μM of glucose, and window of the linear response range, the optimized responses of the 150 and 200 nm $Ni(OH)_2$-NND electrodes were obtained at 0.5 and 0.525 V, respectively. From the results obtained with the 50 to 250 nm $Ni(OH)_2$-NND electrodes, the optimal working potential shifts to higher values but in the case of the 250 nm $Ni(OH)_2$-NND electrode, no distinct linear response was acquired even at the preferred potential. This means that the acceptable range of applied potential gets narrower with increasing Ni thickness.

In general, the effects of applied potential on the amperometric response of the present sensors are similar to those reported in the literature. Taking 100 nm $Ni(OH)_2$-NND (the optimal applied potential is 0.5 V) as an example, the current response increases at a slower rate after a concentration of 1 mM at the lower working potentials of 0.45 and 0.475 V. This is because the electrocatalytic sites on the electrode surface that are driven by low potential are insufficient to instantly electro-oxidize glucose at higher concentrations. However, the background current increases sharply when applying higher potentials. It can be seen that at the potential of 0.55 V, the detection response is poor at lower concentrations but gets better at higher concentrations owing to the competition between electrolysis of water and electrocatalysis of glucose.

The optimal working potential and the corresponding performance for each of the $Ni(OH)_2$-NND sensors with different Ni thicknesses are summarized in Table 1. It is noted that the sensitivity of the sensors improves with increasing Ni thickness until 150 nm and then declines. From the reported research on kinetically controlled electrochemical events as glucose oxidation, it is well-known that the Faradaic current depends on the

Table 1 Determined parameters for electrocatalytic oxidation of glucose on the different Ni thickness coated $Ni(OH)_2$-NND electrodes. Each response represents the mean ± S.D. of five determinations

Ni thickness (nm)	Optimum working potential (V)	Sensitivity (mA mM^{-1} cm^{-2})	Linear range (mM)
50	0.45	2.20 ± 0.14	0.2–1.5
100	0.5	3.10 ± 0.09	0.2–1.8
150	0.5	3.20 ± 0.10	0.2–2.4
200	0.525	2.10 ± 0.10	0.2–2.4
250	0.55	2.10 ± 0.05	0.2–2.0

nanoscopic surface area rather than the geometric surface area of the electrode, especially at slower scan rates. As revealed in Fig. 2(d) and (e), both 100 and 150 nm $Ni(OH)_2$-NND offer sponge-like morphology with extremely large surface, and show enhanced Faradaic currents for electro-oxidation of glucose with higher sensitivities of 3.1 and 3.2 mA mM^{-1} cm^{-2}, respectively. In contrast, the 200 nm $Ni(OH)_2$-NND electrode has quasi-flat morphology (Fig. 2(f)) and exhibits a lower sensitivity of 2.1 mA mM^{-1} cm^{-2}. Thus, the decrease of sensitivity in the 200 and 250 nm Ni-NND electrodes could be attributed to a lack of nanostructured morphology which makes these $Ni(OH)_2$-NNDs behave more like two-dimensional Ni plated electrodes. The most sensitive detection was found with the 150 nm $Ni(OH)_2$-NND electrode owing to the greater number of $Ni(OH)_2$ nanoparticles on the surface. As described in the literature,[14] this is because of the highly distorted line of diffusion flux constructed near the nanostructured electrode surface, the so-called heterogeneous kinetics limitation. Therefore, the 150 nm Ni-NND electrode with a greater surface area, microporous roughness, and $Ni(OH)_2$ decorated nanoparticles generated higher Faradaic currents for glucose oxidation.

Fig. 4(a) displays the amperometric response of the 150 nm $Ni(OH)_2$-NND electrode to successive increments of different concentrations of glucose at the desired operating potential of 0.48 V. With each addition of glucose, the response time was found to be 3 s or less and the steady-state reaction was reached in ~10 s. The corresponding calibration plot is shown in Fig. 4(b). Clearly, the sensor displays two linear ranges, from 0.02 to 1 mM (see inset for details) and from 1 to 9 mM, with different sensitivities of 3.2 and 1.41 mA mM^{-1} cm^{-2}, respectively. The experimental limit of detection was estimated to be 1.2 μM at a signal-to-noise ratio of 3. The phenomenon of two linear regions in glucose response has been reported previously.[38,39] In our case, it can be attributed to the accumulation of the electro-inactive intermediate, glucolactone, near the surface of the electrode. Since the measurements were conducted without stirring, such an accumulation could occur after a period of detection. Owing to the kinetics-controlled mechanism, the transport of glucose to the electrode surface could be slowed down by non-dispersed glucolactone acting as a diffusion barrier, thereby resulting in a severe decrease in the oxidation current responses.

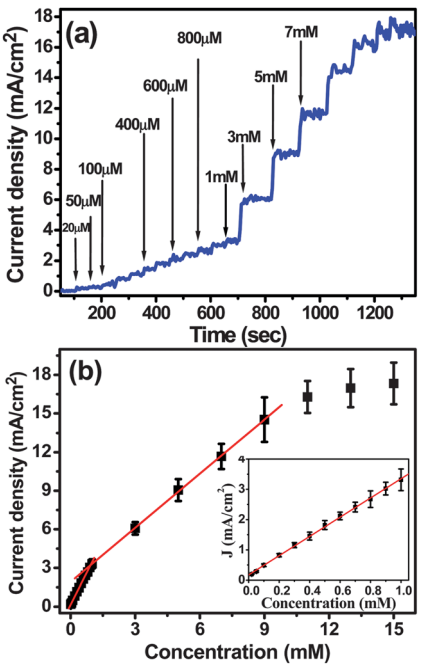

Fig. 4 (a) Amperometric response and (b) the corresponding calibration plot of the 150 nm $Ni(OH)_2$-NND electrode for successive additions of 20, 30, 50, 100 μM, and 2 mM glucose at a potential of 0.48 V in 0.5 M NaOH solution. Each response in (b) represents the mean ± S.D. of five determinations. The inset in (b) depicts the calibration curve in the lower detection range of 0.02–1.0 mM.

Interference study

While analyzing glucose in blood samples, ascorbic acid (AA), acetaminophen (AC), and uric acid (UA) are key species that interfere with the detection of glucose. The normal physiological level of glucose is 4.4–6.6 mM which is several times higher than the concentrations of interfering species, 0.125 mM for AC, 0.13 mM for AA, and 0.3 mM for UA.[40,41] Thus, the interference study was conducted with a starting concentration of 1 mM for glucose and a fixed concentration of 0.1 mM for the interfering species by amperometry at an applied potential of 0.48 V with the 150 nm $Ni(OH)_2$-NND electrode. As shown in Fig. 5, the biosensor exhibited an essentially negligible response toward each addition of the three species in 1 mM glucose and maintained good linear response to successive additions of 2 mM glucose. The corresponding oxidation current density of 1 mM glucose is ~2.5 mA cm^{-2}, which greatly exceeds those recorded for the interfering species: ~0.017 mA cm^{-2} for UA, ~0.13 mA cm^{-2} for AC, and ~0.28 mA cm^{-2} for AA.

The cyclic voltammetric behaviors of different concentrations of glucose and interfering species, AA, AC and UA in 0.5 M NaOH at a scan rate of 10 mV s^{-1} were also investigated. The resulting CVs and calibration curves are shown in Fig. S4 and S5,† respectively. The results show that the sensitivities produced by glucose, AA, AC and UA are 1.25, 0.16, 0.13, and 0.105 mA mM^{-1} cm^{-2}, respectively, confirming the good selectivity of the sensor.

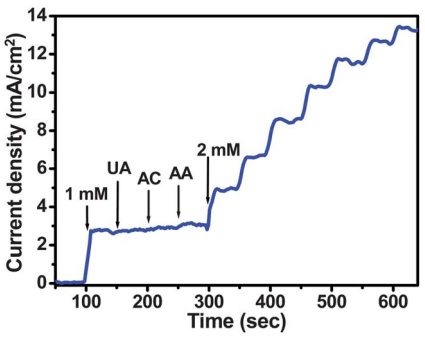

Fig. 5 Amperometric response of the 150 nm $Ni(OH)_2$-NND electrode to 1 mM glucose and successive additions of 2 mM glucose in the presence of 0.1 mM UA, AC and AA at an applied potential of 0.48 V.

From the literature,[42–44] the Ni-based electrodes exhibit excellent electro-catalytic ability to functional groups such as hydroxyl groups (–OH), carboxyl groups (–COOH), and aldehyde groups (–CHO), but are less active to amino groups (–NH). For glucose and AA, the main functional groups that can be oxidized at relatively lower potentials are one primary –OH (1°-OH), four secondary –OH (2°-OH), and one –CHO in each glucose molecule, and one 1°-OH and one 2°-OH in each AA molecule. The –CHO and –COOH groups exhibit better reaction rates than –OH. Therefore, if 1°-OH is oxidized to –CHO, the –CHO group will be rapidly oxidized to the –COOH group. On the other hand, if all the –OH and –CHO groups are oxidized in the first electro-oxidation process, the intermediate having one –CHO and one –COOH group is further oxidized to the other intermediate with one –COOH remaining. Since the 1°-OH and 2°-OH of AA molecules can only carry out three oxidation steps, which oxidize the 1°-OH and 2°-OH to carboxylic groups and carbonyl groups, the current signal of AA received by the $Ni(OH)_2$-NND electrode is inferior to glucose which requires at least seven steps. As for AC and UA, the ring structure and multi-bonds between carbons confine the oxidation of –OH and –NH groups. As a result, the $Ni(OH)_2$-NND electrode exhibits much less current response to AC and AA. That is, the signals of AA, AC and UA are all overwhelmed by the dominant electro-oxidation reaction rate of glucose at the $Ni(OH)_2$-NND electrodes according to their different molecular structures.

Long-term stability

The 150 nm Ni-NND sensor was evaluated for its shelf-life stability. Fig. 6 depicts the amperometric responses of the sensor for detection of 0.5 mM glucose in 0.5 M NaOH at the desired operating potential of 0.48 V after storing in air under ambient conditions for different time-spans. The response of the sensor to 0.5 mM glucose decreased to 85% of its initial value (as deposited one) after 30 days of exposure and then approached a steady response value, which shows good long-term stability. This performance is superior to the $Ni(OH)_2$-modified boron-doped diamond ($Ni(OH)_2$-BDD) sensor proposed by Toghill *et al.* in 2010,[22] which exhibited a response loss of 94% of the initial measurement in just two weeks due to the poor adhesion between the $Ni(OH)_2$ and BDD substrate. The surface bonded structure of BDD, as discussed in the literature, demonstrates p-type features, which provide vacant orbitals to charges and drive the reactions. Contrarily, the surface bonded structure of NND shows n-type states, which means the surface of NND is negative-charge carrier dominated. When comparing the two diamond supporting materials, $Ni(OH)_2$ exhibited much better adhesion to the NND which might be attributed to the interaction between the n-type states and Ni atoms.

Comparison with $Ni(OH)_2$-graphite and other non-enzymatic electrodes

The excellent performance of the 150 nm $Ni(OH)_2$-NDD electrodes toward glucose sensing has been attributed to its highly nanostructured surface. To verify this, another carbon-based supporting material, graphite, was similarly modified with the same 150 nm-thick Ni followed by the same $Ni(OH)_2$ growth process discussed previously. Fig. S6† shows a FESEM image of the 150 nm $Ni(OH)_2$-graphite electrode. A comparison of the amperometric response of both electrodes, the 150 nm $Ni(OH)_2$ modified NND and graphite, to successive additions of glucose at the desired operating potential of 0.48 V can be seen in Fig. 7(a). It can be observed that a much significant current response is obtained at the $Ni(OH)_2$-NND electrode. As indicated from the resulting calibration plots, Fig. 7(b), the $Ni(OH)_2$-NND electrode shows a sensitivity of 3.18 mA mM^{-1} cm^{-2}, which is three times greater than the $Ni(OH)_2$–graphite electrode. This can be explained by the difference in their active surface areas due to the unique microstructure of NDD as seen in Fig. 2(e). Nevertheless, both electrodes display the same linear range from 0.02 to 1 mM, indicating a similarity in their

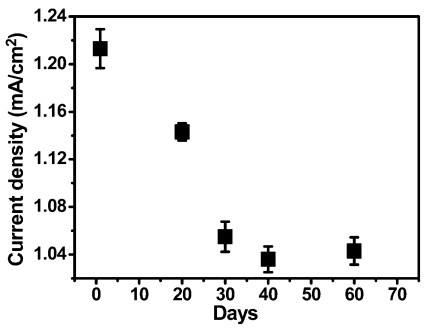

Fig. 6 Stability of the amperometric response of the 150 nm $Ni(OH)_2$-NND electrode to 0.5 mM glucose in 0.5 M NaOH solution for 60 days. Each response represents the mean ± S.D. of five determinations.

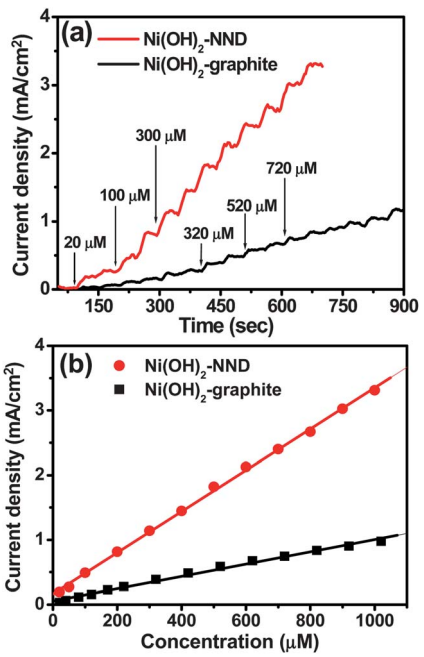

Fig. 7 (a) Amperometric responses of the 150 nm $Ni(OH)_2$-NND and $Ni(OH)_2$-graphite electrodes to successive additions of glucose in 0.5 M NaOH solution at an applied potential of 0.48 V. (b) The corresponding calibration plots.

Table 2 Comparison of the performance parameters of various non-enzymatic glucose sensors[a]

Electrode	Sensitivity ($\mu A\ mM^{-1}\ cm^{-2}$)	Linear range	Detection limit (μM)	Long-term stability	Ref
Ni nanoflake/Ti plate	7320	0.05–0.6 mM	1.2	1 year	15
NiO NP/carbon paste	5590	1–110 μM	0.16	—	17
Ultrathin Ni film/NPG	5070.9	1 μM to 10 mM	—	—	20
NiO NP/MWCNTs	1768.8	0.01–7 mM	2	—	23
Pt NP/MWCNTs	1100	2–20 mM	—	—	45
Ni nanowire array/GC	1043	0.5 μM to 7 mM	0.1	65 days (7% loss)	16
$Ni(OH)_2$/BDD	1040	0.01–10 mM	2.7	14 days (94% loss)	22
Pillar-like Cu/ITO	699.45	1 μM to 0.5 mM	0.5	60 days (15% loss)	46
CuO nanofibre paste/GC	431.3	6 μM to 2.5 mM	0.8	—	47
Ni NPs/C fiber mixture	420.4	2 μM to 2.5 mM	1	—	48
CuO nanospheres GC^{-1}	404.5	Up to 2.55 mM	1	—	49
NiO microfiber/FTO	1785.41	1–270 μM	0.033	30 days (4% loss)	50
$Ni(OH)_2$/NND	a. 3200 b. 1406	a. 0.02–1 mM b. 1–9 mM	1.2	60 days (15% loss)	This work

[a] NP: nanoparticles; NPG: nanoporous gold; MWCNTs: multi-wall carbon nanotubes; GC: glassy carbon; BDD: boron-doped diamond; ITO: indium-doped tin oxide; FTO: fluorine tin oxide; and NND: nitrogen-doped nanodiamond;— not reported.

electrocatalytic abilities. Table 2 further compares the analytical performance of the 150 nm $Ni(OH)_2$-NND electrode for glucose detection with several efficient non-enzymatic electrodes. It can be observed that the proposed $Ni(OH)_2$-NND electrode in this research is superior to most electrodes in terms of sensitivity, linear calibration range, limit of detection and long-term stability.

Conclusion

An enzyme-free amperometric biosensor with excellent electrocatalytic ability for glucose oxidation has been developed. The sensor was based on nanoscale $Ni(OH)_2$ modified NND grown directly on Si substrates. The fabrication scheme is simple and the sensors can be batch fabricated. The electrochemical oxidation mechanism of glucose on $Ni(OH)_2$-NND was investigated and showed kinetically controlled behavior for different Ni thicknesses. The sensitivity of the sensor generally increases with increasing nickel thickness until optimum coverage of nanostructured $Ni(OH)_2$ on NND is reached. Our results indicate that the optimized $Ni(OH)_2$-NND electrode can enhance electrocatalytic ability and long-term stability for glucose detection significantly. Since diamond is chemically stable and biocompatible, further examination of the $Ni(OH)_2$-NND electrode for *in vivo* and *in vitro* applications is in progress. This preliminary finding reveals the possibility of exploiting the NND as an electrochemical biosensor platform whereby high performance addressable sensor arrays with high selectivity, sensitivity, and stability could be built by selective surface modification of the NND platform using a non-enzymatic approach.

Acknowledgements

This work was supported by the "Toward World-Class Universities Project, Centers of Excellence" of the National Tsing Hua University.

References

1 G. G. Guilbault and G. J. Lubrano, *Anal. Chim. Acta*, 1973, **64**, 439.
2 Y. B. Vassilyev, O. A. Khazova and N. N. Nikolaeva, *J. Electroanal. Chem.*, 1985, **196**, 105.
3 R. A. Wilson and P. F. Turner, *Biosens. Bioelectron.*, 1992, **7**, 165.
4 Y. Lin, F. Lu, Y. Tu and Z. Ren, *Nano Lett.*, 2004, **4**, 191.
5 N. Zhang, T. Wilkop, S. Lee and Q. Cheng, *Analyst*, 2007, **132**, 164.
6 D. R. S. Jeykumari and S. S. Narayanan, *Biosens. Bioelectron.*, 2008, **23**, 1404.
7 Y. S. Chen, J. H. Huang and C. C. Chuang, *Carbon*, 2009, **47**, 3106.
8 Z. J. Liu, B. H. Liu, M. Zhang, J. Kong and J. Deng, *Anal. Chim. Acta*, 1999, **392**, 135.
9 K. E. Toghill and R. G. Compton, *Int. J. Electrochem. Sci.*, 2010, **5**, 1246.
10 M. B. Jensen and D. C. Johnson, *Anal. Chem.*, 1997, **69**, 1776.
11 J.-S. Ye, Y. Wen, W. D. Zhang, L. M. Gan, G. Q. Xu and F.-S. Sheu, *Electrochem. Commun.*, 2004, **6**, 66.
12 D. Luo, L. Wu and J. Zhi, *ACS Nano*, 2009, **3**, 2121.
13 C. Chou, J. Chen, C. Tai, I. Sun and J. Zen, *Electroanalysis*, 2008, **20**, 771.
14 Y. Bai, Y. Sun and C. Sun, *Biosens. Bioelectron.*, 2008, **24**, 579.
15 Q. Yi, W. Huang, W. Yu, L. Li and X. Liu, *Electroanalysis*, 2008, **20**, 2016.
16 L.-M. Lu, L. Zhang, F.-L. Qu, H.-X. Lu, X.-B. Zhang, Z.-S. Wu, S.-Y. Huan, Q.-A. Wang, G.-L. Shen and R.-Q. Yu, *Biosens. Bioelectron.*, 2009, **25**, 218.
17 Y. Mu, D. Ji, Y. He, Y. Miao and H. L. Wu, *Biosens. Bioelectron.*, 2011, **26**, 2948.
18 S. J. Park, T. D. Chung and H. C. Kim, *Anal. Chem.*, 2003, **75**, 3046.
19 J. Yuan, K. Wang and X. Xia, *Adv. Funct. Mater.*, 2005, **15**, 803.
20 J. F. Huang, *Chem. Commun.*, 2009, 1270.

21 L. Li and W. Zhang, *Microchim. Acta*, 2008, **163**, 305.
22 K. E. Toghill, L. Xiao, M. A. Phillips and R. G. Compton, *Sens. Actuators, B*, 2010, **147**, 642.
23 W. D. Zhang, J. Chen and L. C. Jiang, *Microchim. Acta*, 2010, **168**, 259.
24 S. Alwarappan, C. Liu, A. Kumar and C.-Z. Li, *J. Phys. Chem. C*, 2010, **114**, 12920.
25 Y.-S. Chen and J.-H. Huang, *Biosens. Bioelectron.*, 2010, **26**, 207.
26 C. G. Specht, O. A. Williams, R. B. Jackman and R. Schoepfer, *Biomaterials*, 2004, **25**, 4073.
27 Q. A. Williams, M. Nesladek, M. Daenen, S. Michaelson, A. Hoffman, E. Osawa, K. Haenen and R. B. Jackman, *Diamond Relat. Mater.*, 2008, **17**, 1080.
28 S. Raina, W. P. Kang and J. L. Davidson, *Diamond Relat. Mater.*, 2008, **17**, 896.
29 S. Raina, W. P. Kang and J. L. Davidson, *Diamond Relat. Mater.*, 2009, **18**, 574.
30 S. Raina, W. P. Kang and J. L. Davidson, *Diamond Relat. Mater.*, 2010, **19**, 256.
31 R. Barnard, C. F. Randell and F. L. Tye, *J. Appl. Electrochem.*, 1980, **10**, 109.
32 H. Bode, K. Dehmelt and J. Witte, *Electrochim. Acta*, 1966, **11**, 1079.
33 R. S. S. Guzman, J. R. Vilche and A. J. Arvia, *J. Appl. Electrochem.*, 1978, **8**, 67.
34 P. Oliva, J. Leonardi, J. F. Laurent, C. Delmas, J. J. Braconnier, M. Figlarz, F. Fievet and A. D. Guibert, *J. Power Sources*, 1982, **8**, 229.
35 A. Safavi, N. Maleki and E. Farjami, *Biosens. Bioelectron.*, 2009, **249**, 1655.
36 P. F. Luo, T. Kuwana, D. K. Paul and P. M. A. Sherwood, *Anal. Chem.*, 1996, **68**, 3330.
37 C. Z. Zhao, C. L. Shao, M. H. Li and K. Jiao, *Talanta*, 2007, **71**, 1769.
38 L. Q. Rong, C. Yang, Q. Y. Qian and X. H. Xia, *Talanta*, 2007, **72**, 819.
39 J. C. Ndamanisha and L. Guo, *Bioelectrochemistry*, 2009, **77**, 60.
40 G. Reach and G. S. Wilson, *Anal. Chem.*, 1992, **64**, A381.
41 S. Hrapovic, Y. Liu, K. B. Male and J. H. T. Luong, *Anal. Chem.*, 2004, **76**, 1083.
42 A. Kowal, S. N. Port and R. J. Nichols, *Catal. Today*, 1997, **38**, 483.
43 R. M. V. Effen and D. H. Evans, *J. Electroanal. Chem.*, 1979, **103**, 383.
44 R. P. Deo, N. S. Lawrence and J. Wang, *Analyst*, 2004, **129**, 1076.
45 D. Rathod, C. Dickinson, D. Egan and E. Dempsey, *Sens. Actuators, B*, 2010, **143**, 547.
46 F. Sun, L. Li, P. Liu and Y. Lian, *Electroanalysis*, 2011, **23**, 395.
47 W. Wang, L. Zhang, S. Tong, X. Li and W. Song, *Biosens. Bioelectron.*, 2009, **25**, 708.
48 Y. Liu, H. Teng, H. Hou and T. You, *Biosens. Bioelectron.*, 2009, **24**, 3329.
49 E. Reitz, W. Jia, M. Gentile, Y. Wang and Y. Lei, *Electroanalysis*, 2008, **20**, 2482.
50 F. Cao, S. Guo, H. Ma, D. Shan, S. Yang and J. Gong, *Biosens. Bioelectron.*, 2011, **26**, 2756.

